

# Diffusive Shock Acceleration in Oblique MHD Shocks: Comparison with Monte Carlo Methods and Observations

Hyesung Kang

*Department of Earth Sciences, Pusan National University, Pusan 609-735, Korea; e-mail:*  
*kang@astrophys.es.pusan.ac.kr*  
*and*

T. W. Jones

*Department of Astronomy, University of Minnesota, Minneapolis, MN 55455; e-mail:* *twj@astro.spa.umn.edu*

## ABSTRACT

We report simulations of diffusive particle acceleration in oblique magnetohydrodynamical (MHD) shocks. These calculations are based on extension to oblique shocks of a numerical model for “thermal leakage” injection of particles at low energy into the cosmic-ray population. That technique, incorporated into a fully dynamical diffusion-convection formalism, was recently introduced for parallel shocks by Kang & Jones (1995). Here, we have compared results of time dependent numerical simulations using our technique with Monte Carlo simulations by Ellison, Baring & Jones 1995 and with *in situ* observations from the Ulysses spacecraft of oblique interplanetary shocks discussed by Baring *et al.*, (1995). Through the success of these comparisons we have demonstrated that our diffusion-convection method and injection techniques provide a practical tool to capture essential physics of the injection process and particle acceleration at oblique MHD shocks.

In addition to the diffusion-convection simulations, we have included time dependent two-fluid simulations for a couple of the shocks to demonstrate the basic validity of that formalism in the oblique shock context. Using simple models for the two-fluid closure parameters based on test-particle considerations, we find good agreement with the dynamical properties of the more detailed diffusion-convection results. We emphasize, however, that such two-fluid results can be sensitive to the properties of these closure parameters when the flows are not truly steady. Furthermore, we emphasize through example how the validity of the two-fluid formalism does not necessarily mean that *steady-state* two-fluid models provide a reliable tool for predicting the efficiency of particle acceleration in real shocks.

*Subject headings:* Cosmic-Rays— particle acceleration— magnetohydrodynamics

## 1. Introduction

The theory of diffusive particle acceleration at collisionless shocks has been quite successful in explaining many aspects of the cosmic ray (CR) population. These include, for example, the nearly power-law spectrum of the CRs detected at the top of the atmosphere, the relation between the break in the power-law around the  $\sim 10^{14}$  eV knee energy to the maximum energy of the CRs achievable in supernova remnants (SNRs), and, also the non-thermal, power-law electron populations deduced from the radio synchrotron observations of SNRs (Drury 1983; Blandford & Eichler 1987; Berezhko & Krymskii 1988). Although the primitive forms of the theory are very straightforward and robust, the microphysics is actually complex, and there are potentially important simplifying assumptions built into the various versions of the theory. In practice nonlinear interactions between the thermal plasma and the nonthermal (CR) plasma are also often likely to be essential. Furthermore, there are certain key features, such as the processes that inject particles from the thermal plasma into the nonthermal plasma (hereafter, simply “injection”) that are not well understood.

Over the past several years significant strides have been made in direct observational tests of diffusive acceleration theory and in comparisons between theoretical models that are sometimes based on very different approaches. For parallel shocks, in which the ambient magnetic field is aligned with the shock normal, the applicability of diffusive shock theory is now fairly well established. Ellison and collaborators have demonstrated good agreement between Monte Carlo particle shock simulations and measurements at the earth’s bow shock (Ellison, Möbius & Paschmann 1990), as well as between Monte Carlo and hybrid plasma shock simulation techniques (Ellison, *et al.*, 1993). Recently Kang & Jones (1995, Paper I) demonstrated that “continuum transport” approaches based on the diffusion-convection equation also provide good models for the same bow shock measurements and that in parallel shocks such continuum models agree well with both types of particle approaches. Paper I also demonstrated that the time-dependent two-fluid derivative of the diffusion-convection model works well as a dynamical model for these shocks, as long as the necessary closure parameters are properly defined.

Paper I, in addition, contained an important step

for developing a physically-based injection model within the diffusive transport formalism. Particle methods have demonstrated injection to be an integral part of collisionless shock formation (*e.g.*, Jones & Ellison 1991 and references therein). Continuum models for diffusive acceleration, on the other hand, have generally depended for practical reasons on an effective separation of the particle population into distinct thermal and CR components with the former treated by fluid mechanical techniques and the latter by approximate plasma kinetic equation techniques or the energy moment of that equation (*i.e.*, the two-fluid model). Paper I introduced a hybrid model of the standard continuum approach. It creates a virtual “injection pool” of particles that are neither fully thermal nor fully “CR”, but represent the particles leaking out of the thermal population into the CR component. We demonstrated there that this continuum “thermal leakage” injection model could produce good agreement with simulations done using particle techniques and with direct bow shock measurements. We focus our discussion, by the way, on the ionic particle population, rather than electrons, since ions carry most of the momentum flux and seem to capture the greater share of energy in the shock transition, especially among the suprathermal, high energy population. To simplify discussion, we deal only with protons, although the methods being used can also be applied to other ions.

The situation regarding oblique shocks is not so well studied and technically more difficult to model. Quasi-parallel and quasi-perpendicular collisionless shock structures may be quite different (*e.g.*, Kennel, Edmiston & Hada 1985). There are complications in the details of diffusive particle propagation (such as anisotropic diffusion with respect to the magnetic field) and acceleration that derive from the magnetic field geometry (*e.g.*, Jokipii 1987). In addition, the magnetic field can apparently modify and reduce in nonlinear ways the amount of energy that CRs are able to extract from the flow through highly oblique shocks (*e.g.*, Webb, Drury & Völk 1986; Jun, Clarke & Norman 1994; Frank, Jones & Ryu 1994, 1995). As a significant step towards a better understanding of the acceleration physics in oblique shocks Baring, *et al.*, 1995 (BOEF95 hereafter) have extended the Monte Carlo studies to oblique shocks through test-particle simulations in which a gyro-orbit computation was adopted and large-angle scatterings were assumed for the particles. They demonstrated that

Monte Carlo shock models with reasonable scattering properties can match *in situ* observations of oblique interplanetary shocks from the Ulysses spacecraft. Ellison, Baring, & Jones 1995 (EBJ95 hereafter) have applied the same techniques to study the acceleration rates and injection efficiencies in oblique shocks. They confirmed earlier findings from different methods that, for anisotropic diffusion, the acceleration rate for individual particles increases with the magnetic field obliquity (*e.g.*, Jokipii 1987; Frank, Jones & Ryu 1995). Thus, quasi-perpendicular shocks may be capable of generating higher energy particles than quasi-parallel shocks in a given time, even though their net energy extraction efficiencies may be reduced by a strong field. In their Monte-Carlo simulations EBJ95 also saw that the efficiency of “thermal-leakage” injection decreases with the obliquity, making it harder for quasi-perpendicular shocks to generate seed CR particles. They found that the injection rate depends upon the Mach number, field obliquity angle, and strength of Alfvén turbulence responsible for scattering. The last of these enters, because it controls the amount of cross-field diffusion, which in quasi-perpendicular shocks becomes necessary for particles to escape into the upstream region in order to be accelerated. A recent complementary discussion of the characteristics of electron injection at quasi-perpendicular shocks has been provided by Levinson (1996).

The present discussion extends the analysis of Paper I to oblique shocks. We apply our thermal leakage injection model to oblique shocks and make a preliminary comparison with the behaviors reported by EBJ95. In addition we turn the model to the same interplanetary shock measurements presented by BOEF95. These results will provide a useful foundation for future studies of oblique shock physics based on continuum models, and expand on a preliminary report made earlier (Jones & Kang 1995). The plan of the paper is this. In §2 we summarize the comparison between particle and continuum models and how that is important to understanding injection. Section 3 outlines our numerical methods, while §4 presents our results, and §5 provides a summary and conclusion.

## 2. Continuum Models and Particle Injection

In continuum treatments of diffusive shock acceleration, the diffusion-convection equation (equa-

tion 3-1; to be discussed in §3) for the particle momentum distribution is solved along with the dynamic equations for the underlying plasma. They have some distinct practical advantages over Monte Carlo methods, especially in time dependent problems and those that involve complex, or multidimensional flows. There are well developed, robust and relatively inexpensive continuum computational techniques available that can be applied very flexibly, for example. There is a growing literature based on time dependent diffusion-convection equation treatments of quasi-parallel shocks (*e.g.*, Falle & Giddings 1987; Kang & Jones 1991; Kang, Jones & Ryu 1992; Duffy, Drury & Völk 1994). The simpler and much more economical, two-fluid derivative of the diffusion-convection method has seen even greater application in time dependent dynamical problems, because it is practical to use in many complicated situations where suitable numerical gasdynamics methods are suitable (*e.g.*, Drury & Falle 1986; Dorfi 1990, 1991; Jones & Kang 1990, 1992, 1993; Ryu, Kang & Jones 1993; Jones 1993; Jones, Kang & Tregillis 1994). Recently, both of these continuum techniques have been extended to time dependent MHD and oblique shocks (Frank, Jones & Ryu 1994, 1995). Jun, Clarke & Norman (1994) also reported two-fluid results for perpendicular MHD shocks. Because of the wide-spread use of two-fluid methods their validity and limits of applicability take on a particular importance. Paper I as well as some other earlier papers (*e.g.*, Duffy, Drury & Völk 1994) have demonstrated basic validity of the model in quasi-parallel shocks. There are some important caveats, however, as we shall discuss later.

The diffusion-convection equation is based on the assumption that a particle momentum distribution is kept almost isotropic in the local fluid frame by scattering. When particle velocities are much greater than the bulk speed of the plasma motion and scattering is efficient these requirements are very reasonable. It is reassuring, but perhaps not terribly surprising that statistical particle approaches like Monte Carlo and continuum (diffusion-convection) methods agree with each other and with real data in that case. In the opposite limit of random particle speeds less than those associated with bulk motion relative to the shock, the theoretical situation is again tractable. Since charged particles generally are scattered more rapidly at small velocities, we can expect them to be “thermalized” effectively and isotropized with respect to a well-defined mean motion. Then continuum

fluid dynamical computational methods should work well, and statistical methods should be convergent with them. The situation is much more problematic at “intermediate” velocities where particle streaming may be large, and mean free paths are too long to allow scattering to relax the distribution to a thermal form. (Particles sample a range of environments, so that no simple thermal equilibrium is appropriate.) This is the arena of injection, since it includes particles that are capable of becoming CRs through multiple shock crossings. The reality of injection in shocks is not much in doubt (*e.g.*, Jones & Ellison 1991), but despite recent theoretical strides (*e.g.*, Malkov & Völk 1995), the details of injection remain beyond straightforward models. This problem is difficult because nonlinear interactions between particles, resonant hydromagnetic waves and the underlying plasma associated with the shock formation process itself are very complex and yet to be deciphered fully. In that context we seek now only a simple, functional model, but one that captures essential physics of the process. Previous injection schemes within the continuum formalism have generally been based on *ad hoc* assumptions that a fixed fraction of the kinetic energy flux or the total particle flux through the shock are transferred from the “thermal” to the “nonthermal” populations, so our new approach represents a clear step towards reality. There is considerable value in developing a serviceable, but physically based model for injection within the continuum transport paradigm.

The thermal leakage injection model introduced in Paper I is conceptually simple and represents only a small change from previous diffusion-convection methods. As before we simultaneously solve the coupled diffusion-convection/MHD equations. However, in this new technique we follow the entire proton momentum distribution with the diffusion-convection equation, but continuously redistribute the particles at low momenta into a thermal distribution according to the pressure and density solution from the MHD equations. That introduces a population of diffusive particles at intermediate momenta between the thermal particles and those properly termed CR particles. Since they are diffusive those particles can sample the fluid velocity on both sides of the shock, if they are given scattering properties suitably matched to the numerical shock thickness. Those intermediate momentum particles gain energy in a manner that resembles what happens to CRs, but their distribution is directly matched onto the thermal distribution, as

it physically must be. The injection efficiency is determined by the momentum at which this “injection pool” distribution is matched to the thermal distribution. Eventually, we hope to be able to provide an independent model for this matching, but for now, it can be sufficient to show that the model successfully reproduces important physical behaviors for physically reasonable matching conditions.

### 3. Model Description

#### 3.1. Numerical Methods

We follow evolution of the particle distribution with the standard diffusion-convection equation (*e.g.*, Parker 1965; Skilling 1975; Jokipii 1982),

$$\frac{df}{dt} = \frac{1}{3} \vec{\nabla} \cdot (\vec{u} + \vec{u}_w) p \frac{\partial f}{\partial p} + \vec{\nabla} \cdot (\kappa \vec{\nabla} f) - \vec{u}_w \cdot \nabla f, \quad (3-1)$$

where  $f(x, p, t)$  is the isotropic part of the distribution function measured in the convected frame,  $\vec{u} + \vec{u}_w$ , while  $d/dt$  is the total time derivative in the fluid frame,  $\vec{u}$ . The propagation of scattering centers relative to the plasma is represented by  $\vec{u}_w$ . Generally, the scattering centers are assumed to be Alfvén waves resonant with the particles, so  $\vec{u}_w$  represents the center-of-momentum motion of those Alfvén waves. Our simulations assume planar symmetry, so  $\kappa = \kappa(p)$ , termed the diffusion coefficient, is the projection of the spatial diffusion tensor onto the shock normal. That direction is taken to be parallel to the  $x$  axis. Throughout the paper we express momentum,  $p$ , in units of the proton rest mass energy,  $mc^2/c$  ( $= 9.38 \times 10^5 \text{ keV}/c$ ), and the distribution function  $f$  in units of the particle number density, so that  $4\pi \int f p^2 dp = \rho/m$ . We solve equation 3-1 on an Eulerian grid using a second-order combined Lagrangian Crank-Nicholson/monotone-remap scheme whose details can be found in Kang & Jones (1991) and Frank *et al.*, (1995), respectively. The distribution  $f(p)$  is supposed to exist over a range  $p_0 \leq p \leq p_3$  that includes both the thermal distribution and the CR distribution. The thermal distribution expressed in terms of  $g(p) = p^4 f(p)$ , which measures the partial pressure,  $dP/dp$ , has its maximum at  $p_{th} = \sqrt{4\tilde{T}} = \sqrt{4m k_B T}/mc$ , where the gas temperature  $\tilde{T}$  is expressed in units  $mc^2/k_B$ . We will identify those particles dynamically as CRs that satisfy  $p \geq p_2 \gg p_{th}$ , and will establish  $p_2$  below.

The dynamics of the underlying plasma is followed by an explicit, second-order accurate MHD

code based on a conservative up-winded, Total Variation Diminishing (TVD) scheme (Ryu & Jones 1995) that has been modified to include the dynamic effects of the CR pressure (Frank *et al.*, 1995). Readers are referred to their papers for the basic MHD equations and the detailed description of the numerical method. Based on a linear Riemann solver used to compute “up-winded” mass, momentum and energy fluxes at zone boundaries, the code generally captures cleanly all the families of MHD discontinuities. Strong shocks are usually contained within 2 to 3 zones, and other discontinuities within a slightly broader space ( $\sim 4 - 10$  zones, depending on the feature). The code is conservative in the sense that it maintains exact net fluxes through the grid to machine accuracy. The TVD label refers to the manner in which the code avoids introducing physically spurious oscillations by preserving monotonicity in physical flow variables through discontinuities.

There is one addition to the code discussed in Frank *et al.*, (1995); namely, “Alfvén Wave Transport” (AWT) terms, as represented in equation 3-1 by  $\vec{u}_w$ . Those are handled in the same way as discussed by Jones (1993) and Paper I for parallel shocks, with the proviso that  $\vec{u}_w$  aligns with the local magnetic field vector. Additional AWT terms provide for gas heating due to dissipation of the energy transferred *from* CRs (the last term in equation 3-1) to Alfvén waves (thence to the plasma) and also transport of the energy and momentum content within the waves. In the present simulations we have neglected the energy and momentum carried explicitly within the wave field, but have included the energy and momentum passed *through* the wave field (see Jones 1993 for details). The magnetic field in this problem lies within a single plane containing the shock normal direction,  $\hat{x}$ . So, without loss of generality we can define the magnetic field to be within the  $x - z$  plane.

For oblique MHD shocks the diffusion coefficient takes the standard form

$$\kappa = \kappa_{\parallel} \cos^2 \theta + \kappa_{\perp} \sin^2 \theta, \quad (3-2)$$

where  $\parallel$  and  $\perp$  refer to diffusion along and across the magnetic field direction, respectively, and  $\theta = \arctan(B_z/B_x)$ . Following Jokipii (1987), we assume a parallel diffusion coefficient of the form  $\kappa_{\parallel} = \frac{1}{3} \lambda_{\parallel} v$ , with the scattering length,  $\lambda_{\parallel} = N r_g$ , where  $r_g$  is the gyro-radius of a particle and  $v$  is its speed. Then, from standard kinetic theory, the ratio of the parallel to perpendicular components is determined by the

ratio  $N > 1$  as

$$\kappa_{\perp}/\kappa_{\parallel} = [1 + (\lambda_{\parallel}/r_g)^2]^{-1} = (1 + N^2)^{-1}. \quad (3-3)$$

Equation 3-2 can be rewritten as

$$\kappa = [N \cos^2 \theta + (\frac{N}{1 + N^2}) \sin^2 \theta] \kappa_B, \quad (3-4)$$

where  $\kappa_B = \frac{1}{3} r_g v$  is the Bohm diffusion coefficient. The limit  $N \rightarrow 0$  corresponds to Bohm diffusion, where  $\kappa_{\perp} \sim \kappa_{\parallel}$ . Cross-field diffusion is determined in this model by the strength of Alfvénic turbulence, since,  $N \sim E_B/(kE_{wk})$ , where  $E_B$  and  $E_{wk}$  are the total energy density in magnetic fields and the Alfvén wave energy density at the resonant wave number,  $k$ , respectively. When scattering is weak, so that  $N \gg 1$ , there is little cross-field diffusion, whereas strong scattering leads to cross field diffusion comparable to field-aligned diffusion. If  $N$  is a constant, it follows for nonrelativistic particles that  $\kappa \propto p^2$ .

### 3.2. A Numerical Injection Model

As we stressed above, the detailed physics of the injection process is not yet well understood, and diffusive transport models cannot, by themselves, accurately treat the particles directly involved in the process. So, as a practical approximation we assume a simple but reasonable scenario in which a small population of near-thermal particles gain excess energy via interactions with resonant waves and form a suprathermal tail on the Maxwellian distribution in the vicinity of the shock front. They provide the seed particles injected into the CR population. As noted before, in our model the particle distribution over the full range of momenta including the thermal plasma is followed explicitly. Below a certain momentum (in units of  $mc$ ),  $p_1 = c_1 p_{th} = c_1 \sqrt{(4\tilde{T})} = c_1 \sqrt{4mk_B T}/mc$ , chosen high enough to include most of the postshock thermal population, the distribution is forced to maintain a Maxwellian form consistent with the local gas density and pressure determined from the MHD equations. Above  $p_1$  particles are allowed to evolve according to the diffusion-convection equation, while only for  $p \geq p_2 > p_1$  are they considered dynamically as CRs. Particles between  $p_1$  and  $p_2$ , thus, constitute “candidate” CR particles, because they are not locally thermalized. They can be injected into the CR population by crossing a momentum boundary at  $p = p_2$  through flow compression. Below  $p_1$  particles are compressed adiabatically

(reversibly) by the flow, except within the shock discontinuity, where the shock jump conditions demand that the compression be irreversible. Above  $p_1$ , on the other hand, compression leads to irreversible energy changes in the particles, because diffusion is irreversible. This combination of effects is the source of energy for the particle acceleration, of course.

We emphasize that the distribution function for thermal particles is used only to provide the reference population needed to match onto the intermediate population, while the thermal pressure,  $P_g$ , is included and handled through the MHD equations. On the other hand, the intermediate population only provides the seed particles for CR particles and has no dynamical effects on the flow in our method. Although the particle distribution is continuous over the full range of momenta, in continuum treatments short of a full solution to the Boltzmann equation one needs to separate the pressure due to thermal particles ( $P_g$ ) and that due to CR particles ( $P_c$ ), because their dynamical behaviors are different. This, of course, necessitates a definition for the CR population. We have done that by choosing  $p_2$  as the arbitrary boundary. At early stages of acceleration, when the particle distribution is almost Maxwellian, the small CR pressure is sensitively dependent upon the chosen value of  $p_2$ , but  $P_c$  is dynamically insignificant then. On the other hand, When  $P_c$  becomes large enough to be important, it becomes much less dependent upon  $p_2$ , because particles of much higher energy dominate the CR pressure. As a result, our calculations are not critically dependent upon the parameter  $p_2$ . So, it is most convenient numerically to fix the value of  $p_2 \sim (3 - 4)p_{th,i}$ , where  $p_{th,i}$  is the thermal peak momentum of the postshock gas of the initial pure gasdynamic shock. The particle supply in the intermediate momentum pool is sensitively controlled by the parameter  $p_1$ , since  $f(p_1)$  is part of the exponential tail of the postshock Maxwellian distribution. According to comparison tests with measurements of a parallel occurrence of the earth's bow shock and with shocks computed by "particle" methods (see Paper I), appropriate values of the related scaling parameter,  $c_1 = p_1/p_{th}$ , fall in the very reasonable range  $c_1 = 1.5 - 2$ . Thus the value of  $p_1$  varies in time and space along with the local gas temperature.

The model further requires us to match the numerical shock thickness,  $\delta x$ , to particle scattering properties, since the numerically realized injection rate will depend upon the ratio  $\lambda(p_1)/\delta x$  (see Paper I). Above

$p_1$  particles are formally diffusive, but unless the scattering lengths of these particles projected onto the shock normal,  $\lambda(p) \cos \theta$ , exceed  $\delta x$ , they cannot be effectively accelerated by the Fermi process. On the other hand thermal particles should not be able to cross the shock within a projected scattering length, since they should then not form into a Maxwellian distribution. Hence, the numerical shock must be thicker than the projected scattering length of thermal particles, but thinner than the projected scattering length of CRs. The structure and thickness of *real* shocks will be dependent upon the details of the strength and geometry of the field, degree of turbulence, the strength of the shock, for example. That issue is beyond the scope of this study. The specifics adopted for the numerical shock thickness will be given later for each case. This "thermal leakage" type injection model is rather simple, but, according to the results reported in Paper I, apparently able to capture essential characteristics of real injection processes, provided that one makes a reasonable choice for the free parameter  $p_1$ .

### 3.3. Initial and Boundary Conditions

For our simulations the initial flow is specified by a simple discontinuous MHD shock using standard jump conditions, which can be found from MHD Riemann solutions, for example, (see Ryu & Jones 1995). The shock faces to the right, so that velocities along the  $x$  axis are negative when the shock is nearly at rest in the grid. All of our shocks start at rest in the grid, but those developing dynamically significant CR pressure become temporarily "over-compressed", as expected, causing them to drift slowly to the left. Three fluid parameters are needed to define the shocks. Those can be the sonic Mach number,  $M_1 = u_{1x}/c_{s1}$ , the strength of the upstream magnetic field,  $B_1$  and the upstream obliquity of the magnetic field,  $\theta_1 = \arctan B_{1x}/B_{1z}$ . The sound speed is  $c_{s1} = \sqrt{\gamma P_g/\rho}$ , where  $P_g$  is the gas pressure,  $\rho$  is the gas density and  $\gamma$  is the gas adiabatic index, taken to be  $\frac{5}{3}$ . We also assume that initially the particle distribution function,  $f(p)$ , is Maxwellian everywhere, with a temperature,  $\bar{T} = (P_g m)/(\rho k_B)$ . Thus, there are no CRs initially. They are injected through thermal leakage as part of the process of shock evolution. The above definition of the temperature, which was used in both EBJ95 and BOEF95 implies that the electron pressure is negligible compared to the proton pressure. More recently, Baring *et*

al., 1996 (BOEF96) have recomputed the properties of the Ulysses-observed shocks, including finite electron pressure. Although that has changed some of the shock parameters, it should not alter any of our conclusions. The influence of a finite electron pressure is certainly straightforward to include when warranted.

The MHD variables are assumed to be continuous across the left and right boundaries of the spatial grid. This is a good assumption, since the shock is approximately at rest in the middle of the grid, keeping any gradients in flow variables small near the boundaries. The particle distribution,  $f(x, p)$ , is also assumed to be continuous across the boundaries, which means diffusive particle fluxes vanish there. This no-flux boundary condition is numerically simple and robust for the diffusion-convection equation. It remains reasonable as long as the particles are confined near the shock and away from the boundaries.

The boundary condition for  $f(p)$  just below  $p_0$  is not relevant here, since the distribution is redefined continuously by the Maxwellian function at each time step for  $p < p_1$ . At the highest momentum boundary, we assume  $f(p) = f(p_3)$  for  $p > p_3$ . This condition is not very crucial either, since the divergence of the flow is rare around the shocks in plane-parallel geometry considered here.

## 4. Results

### 4.1. Comparison with Monte Carlo Simulations

EBJ95 have calculated, by test-particle Monte Carlo simulations, the efficiency of injection at oblique shocks as a function of Mach number,  $M_1$ ; field obliquity,  $\theta_1$ ; and the degree of cross-field diffusion (as measured by  $N = \lambda/r_g$ ). They found the injection to be more efficient for lower Mach numbers, for smaller obliquities and for stronger cross-field diffusion (*i.e.*, smaller  $N$ ). In their Fig. 5 they showed the downstream integral density distribution for particles accelerated in strong shocks for a range of obliquity. This information can be compared directly with the particle distribution functions of our simulations. Thus, we chose these shocks as the comparison models and found the value of  $c_1$  for each value of  $\theta_1$  that gives the best fit to their results. The common shock parameters are  $u_{1x} = 500 \text{ km s}^{-1}$ ,  $M_1 = 100$ ,  $N = \lambda/r_g = 100$ , and  $B_1 = 10^{-8} \text{ Gauss}$ . This represents a very strong shock in the limit of weak cross-field diffusion and weak magnetic field. The obliquity values considered

are  $\theta_1 = 0^\circ$ ,  $20^\circ$ ,  $30^\circ$ , and  $35^\circ$ ; so that all are “quasi-parallel” shocks. Larger obliquities were not considered by EBJ95 for this shock system, since CR injection was found to be completely suppressed.

The EBJ95 simulations were test-particle, so for this comparison test only, we turned off the dynamic evolution of the flow and kept the shock structure as the initial discontinuous jump (thus, with no CR pressure feedback, even though our code is designed to include fully the dynamical contributions of the CR). For these test-particle runs the shock thickness is effectively one grid cell. Since the shock thickness should be of order the mean scattering length of the postshock thermal momentum,  $p_{th}$ , we adjust the grid spacing to be this length (*e.g.*,  $\Delta x = \lambda(p_{th}) = N r_g(p_{th})$ ). All physical lengths in this problem scale with  $\lambda(p_{th})$ , so this model for the shock thickness will make the injection process scale with  $N$ . Our comparisons with EBJ95 were with Monte Carlo simulations that did not include AWT, so we turned those effects off for this particular set of continuum transport simulations.

Monte Carlo simulations intrinsically consider a steady state, while our calculations are time-dependent. Fig. 5 in EBJ95 shows the Monte Carlo, integral density distribution up to 1000 keV. In order to make a good comparison we should integrate our simulations for a time comparable to that required to accelerate a thermal particle to  $E > 1000$  keV. In practice, however, these become fairly expensive for cases with smaller obliquity,  $\theta_1$ , because the integration time is longer ( $t_{acc} \propto \kappa$ ), and so a greater spatial length is required to keep the CR particle distribution small at the boundaries. Thus we evolved each shock for a time needed to accelerate particles to  $E \sim$  a few  $\times 100$  keV. That corresponds to  $(t/10^8 \text{ s}) = 12, 8, 6$ , and 4 for  $\theta_1 = 0^\circ, 20^\circ, 30^\circ$ , and  $35^\circ$ , respectively. Fig. 1 shows the resulting particle distributions at the shock position for the times and values of  $\theta_1$  specified above. The cases shown here are the models with  $c_1$  chosen to match the results of EBJ95. The top panel shows  $p^4 f(x_s, p)$ , where  $x_s$  is the shock position. The canonical test-particle distribution is a power-law; in this strong shock case,  $f(p) \propto p^4$ . The distributions shown in Fig. 1, however, are somewhat steeper than this canonical power-law, because the computed momentum range is finite and because the computed time interval does not a real steady state to be achieved. The slopes of pow-law fits of these distributions at  $p \sim 1.5 \times 10^{-2}$ , for example, are

$q \sim 4.06 - 4.1$ , where  $f(p) \propto p^{-q}$ . Following EBJ95, the bottom panel shows the integral of the distribution function above a given kinetic energy, expressed in units of keV; namely,  $n(> E) = 4\pi \int_p^\infty p'^2 f(p') dp'$ , where  $E = mc^2(\sqrt{p^2 + 1} - 1)$ . The bottom panel also includes the analogous results reported by EBJ95 for their simulations.

As mentioned before, our spectra start to cut off above  $E \sim$  a few  $\times 100$  keV, due to limited evolution time, while the steady-state, EBJ95 Monte Carlo results extend to higher kinetic energy values. More recently Ellison, Baring & Jones 1996 (EBJ96) have extended their test-particle simulations to fully dynamical Monte Carlo simulations. In those simulations they included a “Free Escape Boundary” (FEB), which removes particles that propagate “too far” upstream from the shock. That preferentially removes the highest energy particles, since they have the longest scattering lengths. The net result is an energy cutoff that qualitatively resembles the finite-time cutoff observed in the distributions we show in Fig. 1. Notice that the high energy side of the EBJ95 “quasi-thermal” distributions cut off more sharply than Maxwellian. This presumably results from the rapidly increasing rate of thermal particle “leakage” with momentum in the Monte Carlo simulations. Our distribution, on the other hand, is not allowed to deviate from the Maxwellian form below  $p_1$  corresponding to  $E \sim 2$  keV, and we simply match the nonthermal distribution to it. But we see that within an energy factor of 2 or 3 of the thermal peak ( $p_{th} \approx 1.5 \times 10^{-3}$ ,  $E_{th} \approx 1$  keV) our distribution converges fairly well to that found by EBJ95, below the cutoff imposed by finite acceleration time. Thus, on the whole our model shows itself to be a reasonable way to mimic the injection and acceleration processes. It produces a consistent particle spectrum at energies higher than thermal energies, in agreement with the Monte Carlo simulations, even though the details of the injection of suprathermal particles are not included.

The values of  $c_1$  adopted for the test-particle simulations that fit best with EBJ95 results are 1.4, 1.65, 2.0, and 2.3 for  $\theta_1 = 0^\circ$ ,  $20^\circ$ ,  $30^\circ$ , and  $35^\circ$ , respectively. The increasing values of  $c_1$  for higher obliquity are required to reduce the injection rates for those shocks. From Fig. 1 or from EBJ95 Figs 5 & 6 it is apparent that the injection rate decreases by about two orders of magnitude between  $\theta_1 = 0^\circ$  and  $\theta_1 = 35^\circ$  for this Mach number and  $N$  value. In fact, EBJ95 argue within the test-particle picture that above  $\theta_1 \sim 30^\circ$ ,

injection within strong shocks may be completely suppressed in the absence of cross-field diffusion. The reason for the obliquity dependence is that particles propagate along field lines until they scatter, except for a drift along the shock plane that can be eliminated by referring to the so-called de Hoffmann-Teller frame. In strong, oblique shocks  $\tan \theta_2 = r \tan \theta_1$ , where  $\theta_2$  is the downstream field obliquity and  $r$  is the shock compression ratio; that is, the downstream obliquity is greater than the upstream obliquity and downstream particle motions are more nearly along the shock plane. Thus, as the obliquity increases, a relatively larger total particle speed after an initial scattering is needed to enable a particle to “swim upstream” fast enough to re-cross the shock from downstream. This tendency reduces the number of particles available for injection (Baring, Ellison & Jones 1994). In our simulations the same effect is established by higher values of  $c_1$  for higher obliquity. As  $c_1$  increases thermal leakage is reduced, because the number of particles in the injection pool is reduced. From the above explanation it is clear in this model that injection is less sensitive to obliquity when the Mach number is smaller or when the scattering is stronger (that is  $N$  is smaller). EBJ95 found in those situations that the injection rate is also greater. This implies that smaller values of  $c_1$  should be chosen in our model for smaller  $M$  and for smaller  $N$ , since the injection efficiency is mostly controlled by the value of  $c_1$ . However, we do not attempt here to find a quantitative dependence of  $c_1$  on  $M$  or  $N$ , since the information presented in EBJ95 is insufficient for that. Also, the best-fit values of  $c_1$  could vary with the numerical shock thickness. We leave for the future a more detailed analysis of these model properties.

The above simulations, both ours and those in EBJ95, were of a test-particle character. On the other hand, it is clear that the energy represented in the super-thermal particle distributions is a substantial fraction of the total. Thus, test-particle results are not very meaningful as a measure of the properties of real shocks of this kind. This is not surprising, since previous studies of strong gasdynamic CR shocks have found them to be very efficient at transferring energy from the flow to CRs (*e.g.*, Drury & Völk 1981).

To gain some insights into the properties of these shocks when they are constructed self-consistently, we repeated our simulations, but with the fully dynamic version of our MHD/diffusion-convection code. To keep the tests simple we used the same val-

ues of  $c_1$  to model injection as in the test-particle simulations. For an obliquity less than  $20^\circ$ , however, more than 10% of the particle number density is within the CR population (see Fig.1) by the end of the simulation interval, using the injection rates found by EBJ95. So, one more assumption of the MHD/diffusion-convection approach is invalid; namely, that the inertia within the high energy, CR population can be neglected. For this reason we have done dynamic test runs only for  $\theta_1 = 30^\circ$ . For convenience in later discussions we refer to this model shock as *EBJ95-D*. Unlike the test-particle runs where the shock is one cell thick, strong shocks in fully dynamic runs are captured within about two cells in our code. Thus, for these tests the grid is adjusted so that a cell has thickness,  $\Delta x = 0.5\lambda(p_{th})$  in order again to match the numerical shock thickness to the scattering length for thermal particles; *i.e.*,  $\delta x \approx \lambda(p_{th})$ .

Fig. 2 shows the flow structure around the *EBJ95-D* shock at  $t/(10^7 s) = 4, 8$ , and  $12$ , along with the initial MHD shock jump at  $t = 0$ . The frame of reference is chosen so that the shock is at rest without CR modification to the flow. The physical variables are expressed for simplicity in units of the following normalization constants:  $L_o = 5 \times 10^{15}$  cm,  $\rho_o = 1.67 \times 10^{-24}$  g cm $^{-3}$ ,  $u_o = 5 \times 10^2$  km s $^{-1}$ , and  $P_{go} = 4.175 \times 10^{-9}$  erg cm $^{-3}$ . The numerical grid extends from  $0.0$  to  $3.0$  in units of  $L_o$ . Only the region between  $0.0$  and  $2.0$  is shown in the figure, however. The assumed value of  $c_1 = 2.0$ , is the same as for the test-particle run. Predictably, the CR pressure is dynamically important for this shock, so that it has a clear precursor. Similarly, the maximum compression is  $4.6$  instead of the test-particle value of  $4$  and the postshock gas pressure is lower than that of the initial shock. Note at  $t/(10^7 s) = 12$ , that the shock structure is still evolving rapidly and the postshock CR pressure is already about  $30\%$  of the gas pressure. Thus, it is clear that the test particle approximation is not valid even for this obliquity. Since the shock structure has been modified by the CR pressure from the initial shock jump, the shock is moving slowly to the left from the initial position. As time goes on, the modified structure extends downstream (to the left in Fig. 2) due to advection, while the precursor in the velocity and the CR pressure extends upstream via the diffusion of highest energy particles.

Fig. 3 provides a comparison of the particle distribution and the integrated particle density for *EBJ95-D*, as well as the test-particle calculation shown in Fig.

2 with the same initial conditions. We first note that the gas temperature is lower, so the peak momentum of the Maxwellian distribution,  $p_{th}$ , is lower in the dynamic run, as we expect from the lower postshock gas pressure and higher compression shown in Fig. 2. The postshock gas is colder in the dynamic run and so the particles in the thermal tail have smaller  $r_g$ , while the shock numerical thickness is the same length in both runs. Thus they are less likely to be able to cross the shock in the dynamic run than in the test particle run. This will reduce the injection rate in the fully dynamic run. Therefore, we expect for similar reasons that the injection rates in fully dynamic Monte Carlo simulations would decrease from those given in the EBJ95 test particle simulations, especially for small obliquities.

#### 4.2. Comparison with Ulysses Observations

BOEF95 have compared proton distributions measured directly by the Ulysses spacecraft at oblique interplanetary shocks with results from Monte Carlo simulations of similar shocks. The BOEF95 simulations are also test-particle ones. We have adopted the same shock parameters as they obtained, and calculated the time-dependent evolution of the particle distribution functions. Our runs include fully the dynamical feedback of CRs on the shock structure; however, because we are comparing our results with the Ulysses data rather than the Monte Carlo simulations. The resulting CR-induced flow modifications are small enough that we do not expect significant differences in the particle distributions from a comparable test-particle simulation. Similarly, we have included the effects of Alfvén wave transport, since it would presumably be present in the real interplanetary shocks.

BOEF95 have studied two shocks. For the first shock, observed on April 7, 1991, (hereafter *BOEF95-1*) the following properties are assumed: shock velocity,  $V_s = 153$  km s $^{-1}$ , sonic Mach number,  $M_s = 6.9$ ; Alfvénic Mach number,  $M_A = 3.1$ ; upstream field strength,  $B = 30\mu\text{G}$ ; upstream particle density,  $n_1 = 1.756\text{cm}^{-3}$ ; upstream ion temperature,  $T_1 = 3.57 \times 10^4\text{K}$ , and magnetic obliquity,  $\theta_1 = 77^\circ$ . The second shock, which was observed on April 28, 1991 (hereafter *BOEF95-2*) was a bit weaker than the first shock. This shock is initiated with these conditions: shock velocity,  $V_s = 165$  km s $^{-1}$ ; sonic Mach number,  $M_s = 3.9$ ; Alfvénic Mach number,  $M_A = 2.2$ ; upstream field strength,  $B = 20\mu\text{G}$ ; up-

stream particle density,  $n_1 = 0.338 \text{ cm}^{-3}$ , upstream ion temperature,  $T_1 = 1.3 \times 10^5 \text{ K}$ , and magnetic obliquity,  $\theta_1 = 75^\circ$ .

The grid spacing in all runs for these two shock models is set so that  $\Delta x = 1/2r_g(p_{th})$  for the *BOEF95-1* shock, and  $\Delta x = 1/3r_g(p_{th})$  for *BOEF95-2*, independent of the value of  $N$ . Since the shock spreads over 3-4 cells in these relatively weak shocks, the effective numerical shock thickness,  $\delta x \sim (1-2)r_g(p_{th})$ . These values of  $\Delta x$  are necessary to produce particle fluxes matching the observations. For  $\Delta x$  twice these values, for example, particle fluxes are too low to match the observations with any reasonable choices of  $c_1$ . We note below that the best fits to the Ulysses data correspond to  $N = 4$  for *BOEF95-1* and  $N = 9$  for *BOEF95-2*. These shocks are quasi-perpendicular, with  $\theta_1 \approx 75^\circ$  and  $\theta_2 \approx 85^\circ$ , so that as a particle streams a distance  $\lambda$  along a field line, it moves along the shock normal a distance  $\lambda \cos \theta \sim N \cos \theta r_g$  which is  $\sim (1-2)r_g$ . Thus, it makes sense that the required numerical shock thickness,  $\delta x \sim (1-2)r_g(p_{th})$ .

The value of  $p_2$  was fixed at  $3p_{th,i}$ , where  $p_{th,i}$  is the momentum at which the Maxwellian distribution peaks in the downstream region for the initial shock. The CR pressure is small compared to the gas pressure, and consequently not very different from test-particle conditions. Thus, the choice of  $p_2$  substantially affects neither the flow dynamics nor the particle spectrum.

In order to transform the particle distribution function (which is isotropic to lowest order in the local fluid frame) to the particle count rate in the space craft frame, we need to know the velocity of the downstream flow relative to the spacecraft. That velocity is difficult to compute accurately from the information available, so we chose it to match the particle velocity,  $V_{peak} = 500 \text{ km s}^{-1}$  at the peak of the Maxwellian distribution.

Fig. 4 shows the computed and measured omnidirectional particle flux in the spacecraft frame divided by the particle momentum cubed,  $p^3$ , and also the computed particle distribution function for the *BOEF95-1* shock. The filled dots are the Ulysses data taken from Fig. 1 of BOEF95. Our results are shown at  $t = 6$  minutes. For the velocity range  $500 < V_p < 2000 \text{ km s}^{-1}$ , the simulated particle flux has reached nearly steady values from an initial Maxwellian form after 5 minutes. Three values of  $N = \lambda/r_g = 4, 20$  and  $40$  were tried while keeping  $c_1 = 1.6$ . For the fourth run,  $N = 4$  and  $c_1 = 2.0$

were chosen. The grid spacing is the same and so the shock thickness is about the same for all four cases. All except the  $N = 40$  run produce acceptable fits to the Ulysses data, although the  $N = 4$  is somewhat the best. That value of  $N$  was also preferred by BOEF95 from their Monte Carlo simulations. The similar comparison for *BOEF95-2* shock is presented in Fig. 5. The same quantities are plotted as in Fig. 4. Now our results correspond to a shock evolution time,  $t = 10$  minutes. The value of  $c_1$  for the best fit is again 1.6. Three values of  $N$  are compared; namely  $N = 9, 20$  and  $40$ . For a fourth run  $N = 9$  and  $c_1 = 2.0$  were used. As in BOEF95, the simulated particle fluxes seem to agree best with observations when small values of  $N$  are used. Although these calculations include full dynamic effects of CRs, the modification to the flow structure is insignificant as shown in Fig. 6. But the slight reduction in postshock pressure and temperature in dynamic calculations means somewhat smaller injection rate compared to the test-particle simulations. For test-particle simulations, the particle flux shown in Figs. 4-5 could be about 50 % larger than that of dynamic runs for the velocity near  $1000 \text{ km s}^{-1}$ , for example.

While, in both examples, the comparisons of each case with the BOEF95 fluxes are fairly similar, we can see in the  $p^4 f(p)$  plots that smaller  $N$  leads to higher momentum particles at a given time. That is simply due to the fact that smaller  $N$  leads to smaller  $\kappa$  (see equation 3-2), and consequently a smaller acceleration time, since the individual particle acceleration time,  $t_{acc} \propto \kappa$  (see, e.g., Lagage & Cesarsky 1983). The particle flux near and above  $p_1$ , however, increases with the values of  $N$  for three runs with  $c_1 = 1.6$ . The particles have larger mean free paths for larger  $N$  and so have higher probability to cross the shock, since the shock thickness is about the same for all runs. This leads to a higher particle flux in the injection pool and so a higher injection rate. However, the sensitivity to  $N$  is rather weak in our model, compared to that to  $c_1$ , for a given shock thickness and for a given value of  $c_1$ . The  $c_1 = 2.0$  cases produce fewer CRs, but accelerate them to the same momenta as the same  $N$  and  $c_1 = 1.6$  cases. That is because  $c_1 = 2.0$  places the transition from thermal to non-thermal particles farther into the Maxwellian tail of the postshock distribution, and thus, reduces the population of the injection pool. This shows that the injection rate is mostly controlled by the choice of  $c_1$  for a given shock thickness. In our numerical injection

model we do not have a self-consistent way to determine the best value of  $c_1$  for a given value of  $N$ , while in Monte Carlo simulations the injection is treated self-consistently. On the other hand, the fact that the numerical shock thickness must be relatively thin to produce consistent fluxes (*i.e.*,  $\delta x \sim (1-2)r_g(p_{th})$ , so that  $N \cos \theta \sim 1$  for the best fits with  $N$ ) could imply that the observed particle flux cannot be explained if the scattering turbulence is weak (*e.g.*,  $N \gg 1$ ). This is consistent with the conclusions of BOEF95.

Again these comparison calculations have shown that the diffusion-convection formalism with our new injection scheme and a reasonable set of scattering and injection parameters can reproduce the particle injection and acceleration processes in real oblique MHD shocks. The detailed dependence of our calculations upon the model parameters such as  $c_1$  and grid spacing should not be overemphasized, since our model is not intended to represent the detailed microphysics of the injection and shock formation processes, but rather only to try to capture the outcomes reasonably well.

### 4.3. Two-Fluid Comparisons

Beginning from the above successes, it is useful to provide direct comparisons between the diffusion-convection simulations and the simpler two-fluid versions of them. Two-fluid methods have been especially useful in complex time dependent applications, such as the evolution of supernova remnants (*e.g.*, Dorfi 1991; Jones & Kang 1992). They are currently the only practical method of calculating multi-dimensional CR-modified flows (*e.g.*, ). As mentioned in the introduction, there has been some controversy in the past about the conditions under which two-fluid methods can provide reliable dynamical solutions for diffusive shock structures. Paper I addressed some of these issues in the context of parallel shocks, and identifies some of the background literature. We demonstrated there the basic agreement between two-fluid and diffusion-convection methods. Arguments are sometimes expressed that momentum-dependent, cross-field diffusion in oblique shocks could invalidate the fluid-like CR behaviors implicit in the two-fluid formalism. To the best of our knowledge the only previous comparisons of the methods for oblique MHD shocks were by Frank, Jones and Ryu (1995). They considered only a case with a momentum independent diffusion coefficient and one with weak momentum dependence,  $\kappa \propto p^{1/2}$ . Thus, we provide here a similar

comparison as in Paper I, but now for oblique MHD shocks. For this we choose two representative shocks; namely, *EBJ95-D* and *BOEF95-1* described in §4.1 and §4.2, respectively.

In the two-fluid version of the diffusive acceleration model the energy moment of the diffusion-convection equation (3-1) is integrated from  $p_2$  to  $p_3$  to produce the conservation equation for CR energy; namely,

$$\frac{dE_c}{dt} = -\gamma_c E_c (\vec{\nabla} \cdot \vec{u}) + \vec{\nabla} \cdot (\langle \kappa \rangle \vec{\nabla} E_c - \vec{u}_w \gamma_c E_c) \quad (4-1) \\ + \vec{u}_w \cdot \vec{\nabla} P_c + S_{tf},$$

where  $E_c$  is the CR energy density. No new approximations are introduced in deriving equation 4-2 from equation 3-1. It does contain three closure parameters,  $\gamma_c$ ,  $S_{tf}$  and  $\langle \kappa \rangle$  that are really properties of the solution, but in practice must be estimated *a priori*. For these particular simulations it is sufficient to set the CR adiabatic index,  $\gamma_c = \frac{5}{3}$ , since the particle populations are entirely nonrelativistic. The injection energy rate,  $S_{tf}$  represents energy exchange with the thermal plasma (see also equation [2.5] in Paper I). In the diffusion-convection simulations, we calculate numerically an analogous injection energy rate,  $S$ , from the particle flux crossing the low momentum boundary of the CR population at  $p_2$ , and subtract it from the thermal energy. Then the spatially integrated injection rate for the two-fluid model,  $I = \int S dx$ , can be parameterized by a dimensionless two-fluid “injection parameter”,  $\eta$ , through the relation  $I = (1/2)v_2^2 \rho_1 u_1 \eta$  where  $v_2 = p_2 c$  (see equation [2.4] in Paper I). Thus we calculate  $\eta$  rather than  $I$  itself as a function of time for each shock modeled using the results of the kinetic equation calculations. In practice the value of  $\eta$  is fairly constant over time in the cases we have considered, so very comparable two-fluid solutions would be found by assuming a single value in each test; namely  $\eta \approx 0.006$  for *EBJ95-D* and  $\eta \approx 0.002$  for *BOEF95-1*.

To model the mean diffusion coefficient,  $\langle \kappa \rangle$  (see equation [2.13] in Paper I), we used the form for  $\kappa(p)$  discussed in §3 and a simple power-law model for the CR distribution function; namely,  $f(p) \propto p^{-q}$ , where  $q = 3r/(r-1)$  is the standard test-particle index expected for diffusive acceleration and  $r$  is the initial compression ratio for the shock (see Figs. 2, 6). We supposed that the CR distribution extended between  $p_2$ , as defined for the full diffusion-convection simulation and  $p_3$  found from the usual relation between particle energy and mean acceleration time

(Lagage & Cesarsky 1983; EBJ95). In the present context that leads to  $p_3 = p_2(1 + t/\tau)^{1/2}$ , where  $\tau = \frac{3}{2}\kappa(p_2)/(u_1\Delta u)$ , and  $\Delta u = u_2 - u_1$ , for the initial shock. In practice we obtained somewhat better matches with the diffusion-convection runs by replacing the factor  $\frac{3}{2}$  by the factor 2; that is, the distribution begins to cut off a little below  $p_3$ . Our results presented here use that latter value.

Two-fluid models are intended only for dynamical studies, so the appropriate tests are comparisons of shock structures computed by the two-fluid model and structures computed by diffusion-convection methods (or actual shocks, if available). The two-fluid shock structure evolution for *EBJ95-D* is shown by the dotted lines in Fig. 2. The agreement with the diffusion-convection simulation is good, reinforcing our earlier conclusions about the basic validity of the two-fluid model. At the end of this simulation ( $t = 1.2 \times 10^8$  sec)  $P_c$  is definitely producing important modifications to the flow structure. It is still increasing, so that a more major dynamical influence could be expected at later times. In fact, the time asymptotic two-fluid solution for this shock should be completely CR dominated, as can be demonstrated from comparable shock solutions in the Figure 3 presented by Kang & Jones (1990), or Figure 3 of Frank, Jones & Ryu (1995), for example. It is simple to demonstrate that the time-asymptotic two-fluid jump conditions (hence,  $P_c$  downstream), are independent of the value or spatial structure of the diffusion coefficient. For this shock, however, the time required to approach that solution from the initial conditions we used would be extremely long; so long, in fact, that the practical significance of the time-asymptotic solution is doubtful.

By contrast, the shock structure at intermediate times is influenced sensitively by the early time evolution of  $\langle\kappa\rangle$ . That grows quickly and asymptotes to  $\langle\kappa\rangle \propto (t/\tau)^2$ . The rate of dynamical shock evolution generally scales inversely as the “diffusion time”,  $t_d = \langle\kappa\rangle/u_1^2$ . That means at late times the shock structure evolves very slowly. At intermediate times,  $P_c$  is largely controlled by the very early history of the shock; particularly  $\langle\kappa\rangle$  and  $\eta$ . So, the match we see in Fig. 2 between the diffusion-convection and two-fluid simulations is sensitive to the values of  $\tau$  and  $\kappa(p_2)$ . That the appropriate value of  $\tau$  is reasonably well predicted by the simple test particle theory for the diffusion coefficient is an encouraging outcome. The minor differences between the diffusion-convection and

two-fluid runs come, in fact, from small differences in the upstream spatial variations of  $\langle\kappa\rangle$  modeled in the two-fluid calculations and as computed directly from the diffusion-convection simulation. In the diffusion-convection simulation, the particle distribution tends to “harden” significantly upstream of the shock (see, e.g., Kang & Jones 1991; Paper I), so the actual  $\langle\kappa\rangle$  increases away from the shock, reducing the value of  $P_c$  as a result.

The *BOEF95-1* shock has a dynamically very significant magnetic field, so it presents an important comparison case for two-fluid models in the MHD shock context. Both the two-fluid and the diffusion-convection shock structures for *BOEF95-1* are shown in Fig. 6. The two-fluid parameters were determined in exactly the same way as for *EBJ95-D*. Again the agreement between the two models is very good. Recall that we already made a comparison between the particle velocity distributions from the diffusion-convection solution and the Ulysses observations, but that we have no detailed information about the physical, interplanetary shock structure. In this case the value of  $P_c$  at the shock is less than 10% of the gas pressure,  $P_g$ , by the end of the simulations ( $t = 6$  minutes), so there is only minor modification of the shock structure by the CRs. In *BOEF95-1*, as in *EBJ95-D* the structure at intermediate times is primarily determined by the evolution of  $\langle\kappa\rangle$  at the early times in the simulation. Again, because  $\langle\kappa\rangle$  increases rapidly with time, the  $t_d$  that determines the rate of shock evolution becomes very long. A direct consequence of this is that, despite the apparently steady shock by the end of the simulation (and also the diffusion-convection simulation), we are *not* seeing the solution that would be determined from the steady-state two-fluid model.

To illustrate the point, we can take advantage of the argument made earlier that the steady-state jump conditions can be found using any convenient diffusion coefficient. For this we have recomputed *BOEF95-1* using a constant  $\langle\kappa\rangle = 0.4$ , and allowed it to evolve to a steady state. In this case we use the criterion for a time-asymptotic solution that not only does the peak value of  $P_c$  become steady, but also that  $P_c$  be uniform directly behind the shock. The evolution of this shock (*BOEF95-1C*) and its final structure are shown in Fig. 7. Early on, the evolution of *BOEF95-1C* and *BOEF95-1* are similar, because  $\langle\kappa\rangle$  are comparable. However, as the *BOEF95-1* diffusion coefficient increases dynamical evolution “stalls”,

while the constant diffusion coefficient of *BOEF95-1C* allows it to continue directly towards the formal steady state solution. The final acceleration efficiency of this shock as measured by  $P_c$  is more than an order of magnitude greater than for the *BOEF95-1* simulations presented earlier or the physical shock. Thus, it would clearly be inappropriate to apply the steady state two-fluid model to estimate the efficiency expected in this shock for even moderately long times.

The discrepancy is not an indication of basic flaws in the two-fluid model, but rather that time-asymptotic solutions are not very relevant in this situation. The key question becomes how to choose, in the two-fluid model, a meaningful set of closure parameters for a time dependent calculation. In both of the tests conducted here it seems adequate to apply simple test-particle models to those parameters, because the shock structure is not sufficiently modified on short times. Over longer times that convenience may become dubious, but, since the shock properties at moderately late times are largely set by the conditions early in the shock evolution, this breakdown may not be crucial in many instances. It is important to know, then, if the shock structure should evolve quickly on time scales of interest. That is something we can hope to estimate reasonably well using the standard test-particle approach. These issues are more important if we expect a steep momentum dependence to the diffusion coefficient, as in the cases studied here, so a more basic understanding of the evolution of the resonant Alfvén wave field becomes important, as well.

## 5. Conclusion

In order to study the particle acceleration in oblique magnetohydrodynamic (MHD) shocks, we have implemented the existing diffusion-convection methods of Kang & Jones 1991 into a full MHD code, and adopted a “thermal leakage” type injection model introduced by Kang & Jones 1995 (Paper I). In our injection model, the distribution of the suprathermal particles which cannot be treated properly with the diffusion-convection method was assumed to match smoothly onto the Maxwellian distribution of the gas particles. The matching condition is controlled by a free parameter  $c_1$ , which in turn determines the particle injection rate into the CR population. Firstly, we have calculated the MHD shocks for various field obliquities considered by Ellison, Baring & Jones (1995), in order to study the dependence of the

injection efficiency on some shock properties via test-particle Monte Carlo simulations. By adjusting the free parameter  $c_1$  of our injection model over a modest range we were able to demonstrate that our numerical technique can, in fact, produce particle spectra comparable to theirs. Secondly, we have reproduced the proton flux distributions at oblique interplanetary shocks observed *in situ* by the Ulysses spacecraft. These shocks have also been simulated previously by Baring *et al.*, 1995, via test-particle Monte Carlo technique. We adopted the shock parameters chosen by them to match direct observations. To obtain good agreement with the observations, the numerical shock thickness for these quasi-perpendicular shocks has to be about (1-2) times the thermal gyro-radius. This is consistent with the conclusion of Baring *et al.*, that strong scattering turbulence was present in these interplanetary shocks.

The Monte Carlo technique treats both thermal and cosmic ray particles by the same scattering law, so the injection process comes about naturally via the acceleration of thermal particles to higher energies. In contrast, injection cannot be determined self-consistently through diffusion-convection models for cosmic-ray transport, since particles at momenta where injection occurs do not form an isotropic distribution and the diffusion approximation is not valid. Our model works around this by introducing a free parameter that establishes the momentum at which the suprathermal distribution must match onto the thermal distribution behind the shock. One might be concerned that the particle distribution at intermediate energies (between the thermal peak energy and energies much greater than thermal peak energy) would be dependent upon the details of the injection process. Our simulations, however, seem to indicate that the dependence is not sensitive enough to make a clear distinction between the particle spectra simulated with our diffusive injection model and existing observations, or the particle spectra simulated with Monte Carlo techniques. This leads us to the tentative, but encouraging conclusion that a simple, macrophysical model like ours can offer a practical compromise between *ad hoc* injection and injection models built to include microphysical details.

Comparison tests presented here and in Paper I have shown that, in our model, the injection process and its rate are mostly determined by the numerical shock thickness in terms of the thermal gyro-radius and the momentum,  $p_1 = c_1 p_{th}$ , where the

suprothermal particle distribution matches onto the Maxwellian distribution. Presumably both of these are affected in a detailed model by the strength of Alfvén turbulence (e.g., Malkov & Völk 1995). Under the assumption that the shock thickness is about the mean scattering length of the thermal peak momentum,  $p_{th}$ , for quasi-parallel shocks and the thermal gyro radius,  $r_g(p_{th})$  for quasi-perpendicular shocks, the appropriate value of  $c_1$  lies between 1.5-2. A smaller  $c_1$  leads to larger injection rates, because it allows a larger “injection pool” of diffusive particles to form. EBJ95 found in Monte Carlo simulations that the rate of particle injection decreased strongly with increasing obliquity for strong shocks, unless the cross-field diffusion was strong. In our model that is effected by increasing the parameter  $c_1$  with obliquity or decreasing it towards smaller Mach number or stronger Alfvén turbulence. More quantitative prediction requires much further work, however. We note also that the injection efficiencies given in EBJ95, which were based on test-particle simulations, are overestimated compared to dynamical shocks, especially for strong, quasi-parallel shocks, since the CR energy density predicted by those simulations is significant enough that the CRs would modify the shock dynamics. In particular, the thermal particle distribution would be colder and the subshock velocity jump would be smaller in self-consistent dynamic calculations. These differences between test-particle and dynamical shocks were confirmed by the recent Monte Carlo simulations of EBJ96.

In Paper I, we showed that diffusive acceleration numerical methods applied to parallel shocks produce similar shock structures and particle distributions compared to Monte Carlo and hybrid plasma methods, and that they matched direct observations at the earth’s bow shock. The comparisons reported here for oblique shocks strengthen the important conclusions of Paper I that the essential physics of the particle injection and acceleration can be captured by each of these diverse computational methods, and that they are all practical and complementary tools for understanding the physics of diffusive shock acceleration. This also implies that our numerical approach provides a way to incorporate naturally the injection process into the existing diffusion-convection technique. The advantages of this formalism distinguishing it from Monte Carlo or plasma methods are that it is time-dependent, in addition to being a fully dynamically self-consistent MHD diffusion-convection

technique, so that it can be used for evolving and structurally complex flows. In upcoming papers, we will use it to study the acceleration efficiency and the nonlinear back reaction of CR pressure on the shock dynamics in various astrophysical shock waves.

We also simulated a pair of oblique two-fluid shocks. Each was constructed exactly as for one of the diffusion-convection simulations reported, with the required closure parameters determined from simple test-particle considerations. The dynamical properties of the two-fluid shocks are quite consistent with the diffusion-convection solutions. These simulations demonstrate in the oblique shock context the basic validity of the two-fluid method. We emphasize, however, that *steady state* two-fluid solutions may not be applicable, even when the shock structures appear to be steady. If the cosmic-ray diffusion coefficient has a strong momentum dependence, the rate of shock evolution can become very slow, so that while a shock may appear dynamically steady, in practical terms the time-asymptotic solution is not likely to be reached for a long time. Then the dynamical conditions creating the shock may very likely have changed, requiring the shock to readjust once more.

We are grateful to Matthew Baring for illuminating discussions about oblique CR shocks and Monte Carlo methods and for useful suggestions that helped us improve the manuscript. This work was supported in part at the University of Minnesota by the NSF through grant AST-9318959, by NASA through grants NAGW-2548 and NAG5-50505 and by the University of Minnesota Supercomputer Institute. HK is supported in part at Pusan National University by the Korean Research Foundation through the Brain Pool Program.

## REFERENCES

Baring, M. G., Ellison, D. C. & Jones F. C. 1994, ApJS, 90, 547

Baring, M. G., Ogilvie, K. W., Ellison, D. C. & Forsyth, R. 1995, Advances of Space Research, 15, 397 (BOEF95)

Baring, M. G., Ogilvie, K. W., Ellison, D. C. & Forsyth, R. 1996, ApJ, in press (BOEF96)

Berezhko, E. G., & Krymskii, G. F., 1988, Soviet Phys. Usp., 31, 27

Blandford, R. D., & Eichler, D., 1987, Phys. Rept., 154, 1

Dorfi, E. A., 1990, A&A, 234, 419

Dorfi, E. A., 1991, A&A, 251, 597

Drury, L. O'C., 1983, Rept. Prog. Phys., 46, 973

Drury, L. O'C. & Falle, S. A. E. G. 1986, MNRAS, 223, 353

Drury, L. O'C., & Völk, H. J., 1981, ApJ, 248, 344

Duffy, P., Drury, L. O'C., & Völk, H. 1994, A&A, 291, 613

Ellison, D. C., Möbius, E., & Paschmann, G. 1990, ApJ, 352, 376

Ellison, D. C., & Eichler D. 1984, ApJ, 286, 691

Ellison, D. C., Baring, M. G., & Jones, F. C. 1995, ApJ, 453, 873 (EBJ95)

Ellison, D. C., Baring, M. G., & Jones, F. C. 1996, ApJ, (in press) (EBJ96)

Ellison, D. C., Giacalone, J., Burgess D., & Schwartz, S. J. 1993, JGR, 98, 21085

Falle, S. A. E. G., & Giddings, J. R., 1987, MNRAS, 225, 399

Frank, A., Jones, T. W. & Ryu, D. 1995, ApJS, 90, 975

Frank, A., Jones, T. W. & Ryu, D. 1995, ApJ, 441, 629

Harten, A. 1983, J. Comp. Phys., 49, 357

Jokipii, J. R. 1982, ApJ, 255, 716

Jokipii, J. R. 1987, ApJ, 313, 842

Jones, F. C., & Ellison, D. C., 1991, Space Science Reviews, 58, 259

Jones, T. W., 1993, ApJ, 413, 619

Jones, T. W., & Kang, H., 1990, ApJ, 363, 499

Jones, T. W., & Kang, H., 1992, ApJ, 396, 575

Jones, T. W., & Kang, H., 1993, ApJ, 402, 560

Jones, T. W., & Kang, H., 1995, 24<sup>th</sup> ICRC Proceedings (Rome), vol3, 245

Jones, T. W., Kang, H. & Tregillis, I. L. 1994, ApJ, 432, 194

Jun, B., Clarke, D. A., & Norman, M. L. 1994, ApJ, 429, 748

Kang, H., & Jones, T. W., 1990, ApJ, 353, 149

Kang, H., & Jones, T. W., 1991, MNRAS, 249, 439

Kang, H. & Jones, T. W., 1995, ApJ, 447, 944

Kang, H., Jones, T. W. & Ryu, D. 1992, ApJ, 385, 193

Kennel, C. F., Edmiston, J. P. & Hada, T., 1985, in *Collisionless Shocks in the Heliosphere: A Tutorial Review*, ed. R. G. Stone & B. T. Tsurutani (Amer. Geophys. Union: Washington, D. C., p 1

Lagage, P. O. & Cesarsky, C. J., 1983, A&A, 125, 249

Malkov, M. A. & Völk, H. J. 1995, A&A, 300, 605

Parker, E. N., 1965, Planet. Sp. Sci., 13, 9

Ryu, D. & Jones, T. W., 1995, ApJ, 442, 228.

Ryu, D., Kang, H. & Jones, T. W. 1993, ApJ, 405, 199

Skilling, J., 1975, MNRAS, 172, 557

Webb, G. M., Drury, L. O'C. & Völk, H. J. 1986, A&A, 160, 335

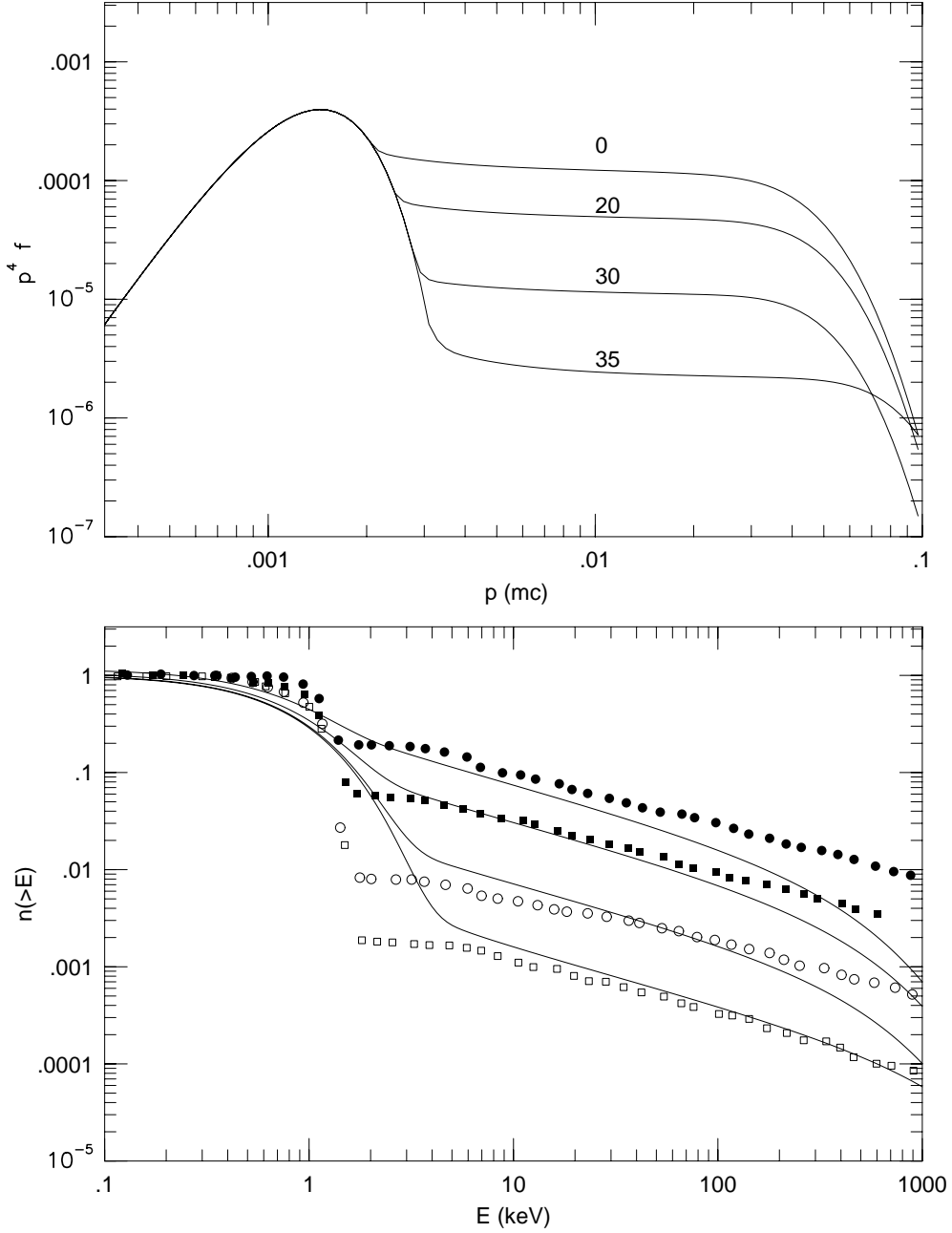


Fig. 1.— Top panel shows the distribution function  $g = f(x_s, p)p^4$  versus the particle momentum  $p$  in units of  $mc$  for particles at the shock for *EBJ95* test runs. The lines are labeled by the value of the upstream obliquity angle  $\theta_1$ . The results are shown at  $(t/10^8 s) = 12, 8, 6$ , and  $4$  for  $\theta_1 = 0^\circ, 20^\circ, 30^\circ$  and  $35^\circ$ , respectively. See text for the shock parameters. Bottom panel shows the integral density distributions calculated from the momentum distribution function shown in the top panel. The open and filled circles and squares are representative points of *EBJ95* Monte Carlo simulation results of the same shock conditions (from their Fig. 5).

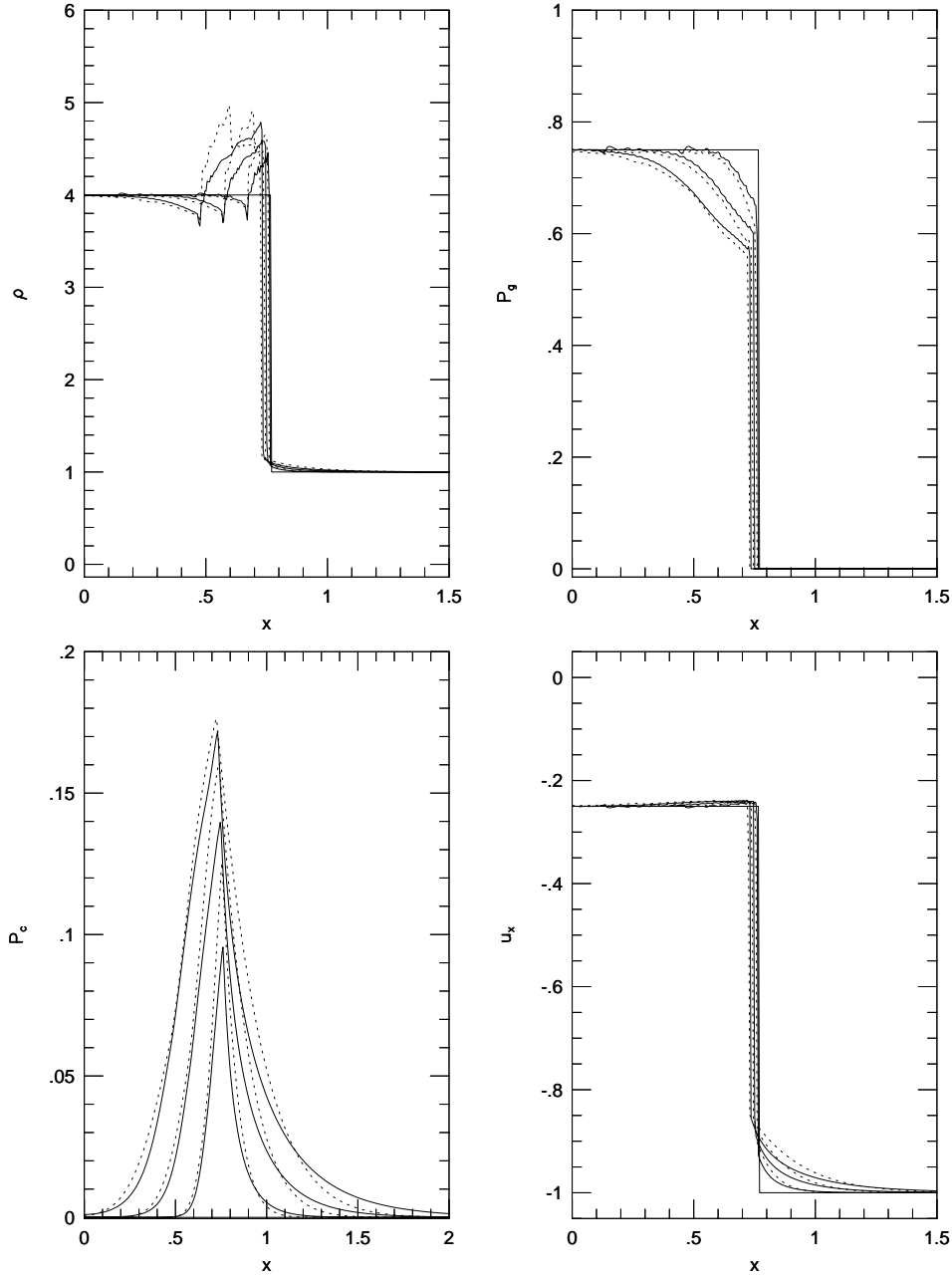


Fig. 2.— The shock flow structure of the model *EBJ95-D* shock at  $(t/10^8s) = 0.4, 0.8, 1.2$  in our fully dynamical simulations (solid line). The initial condition is specified by the pure MHD shock jump. The two-fluid solution for the same shock as discussed in §4.3 is shown by the dotted line. This is a Mach 100 shock, with a very weak magnetic field at an upstream obliquity,  $\theta_1 = 30^\circ$ .

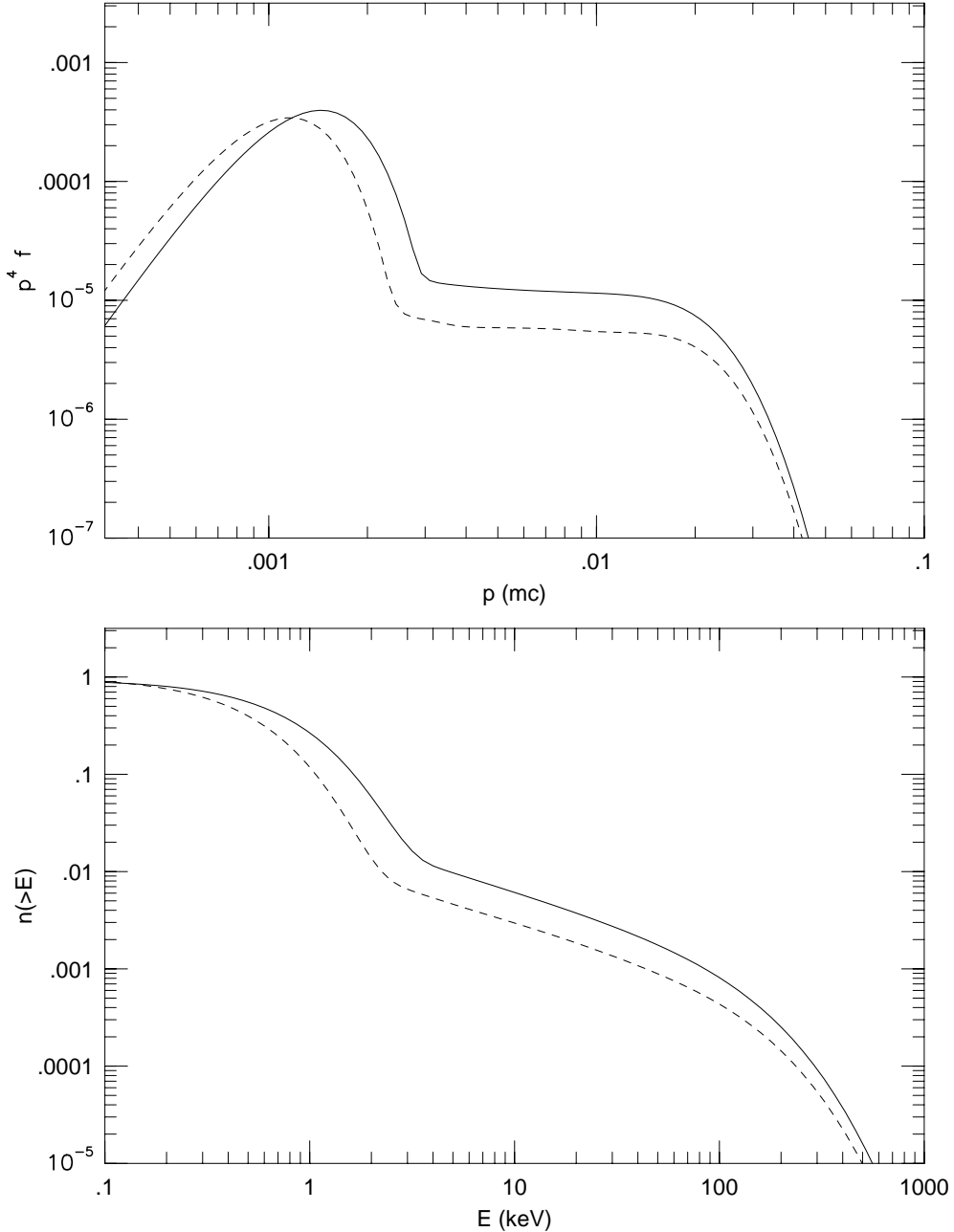


Fig. 3.— Top panel shows the distribution function  $g = f(x_s, p)p^4$  versus the particle momentum  $p$  at the shock for *EBJ95* test runs at  $(t/10^8 s) = 1.2$ . The obliquity,  $\theta_1 = 30^\circ$  and the injection parameter,  $c_1 = 2.0$ . The solid line is the spectrum from the test-particle run, while the dotted of line is for fully dynamic runs. Bottom panel shows the integral density distributions calculated from the distribution functions shown in the top panel.

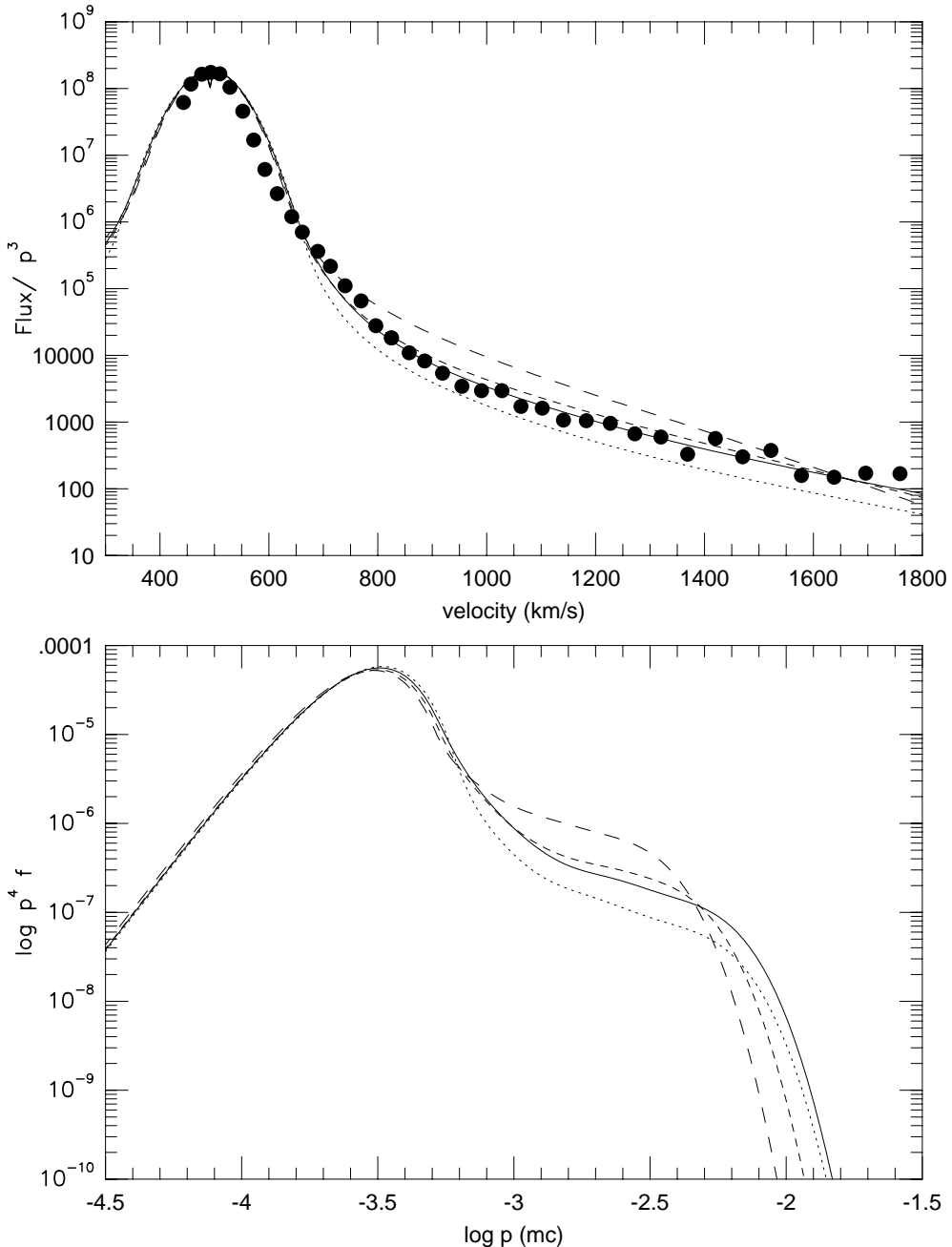


Fig. 4.— Simulated omni-directional particle flux in the Ulysses spacecraft frame divided by the particle momentum cubed,  $p^3$  (upper), and the particle distribution function  $f(p)$  (lower) for BOEF95-1 shock at  $t = 6$  minutes. The solid line is for  $N = 4$ , dashed line for  $N = 20$ , and long-dashed line for  $N = 40$ . The value of  $c_1 = 1.6$  for these three runs. The dotted line is for  $N = 4$  and  $c_1 = 2.0$

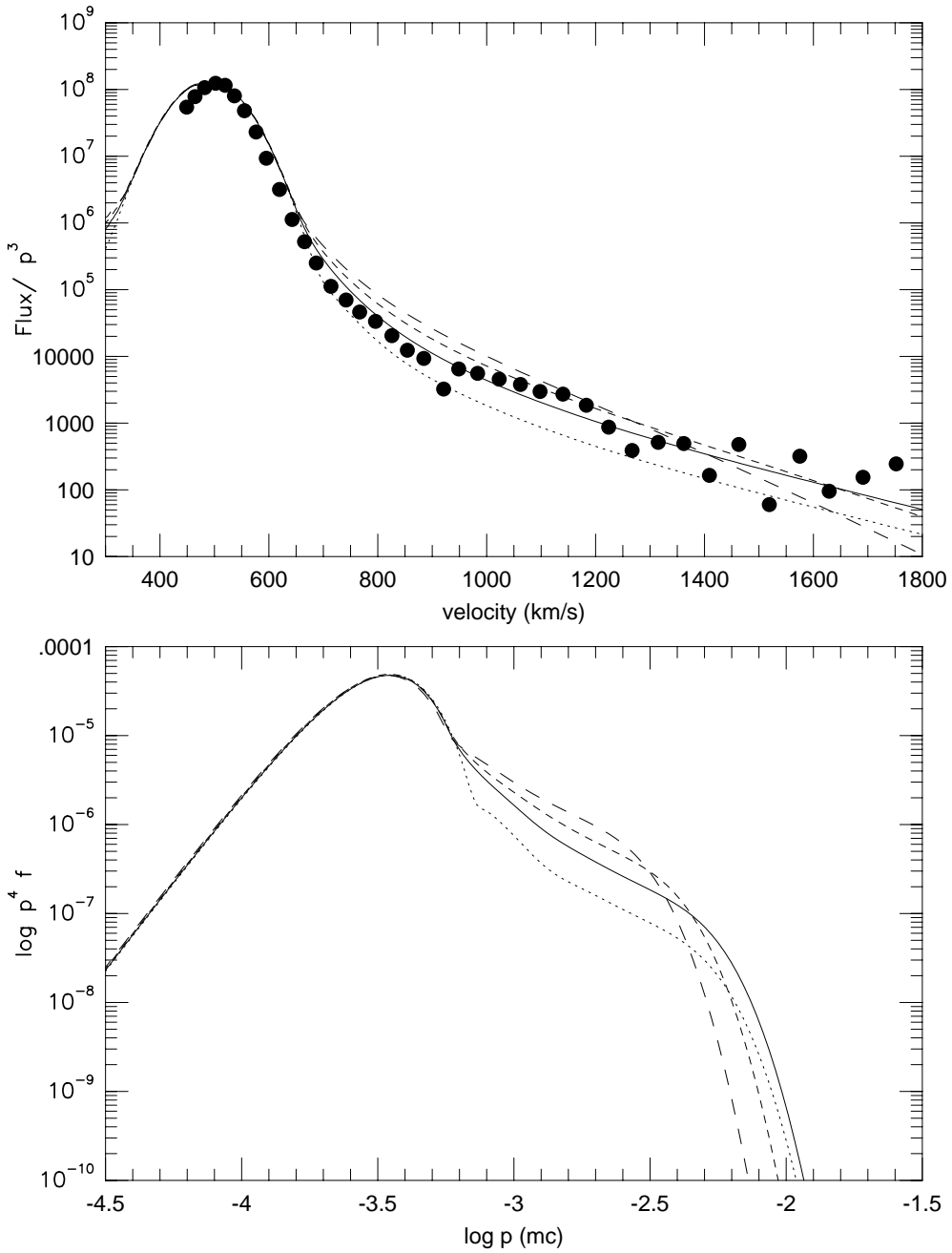


Fig. 5.— Same as Fig. 4, except for *BOEF95-2* shock at  $t = 10$  minutes. The solid line is for  $N = 9$ , dashed line for  $N = 20$ , and long-dashed line for  $N = 40$ . The value of  $c_1 = 1.6$  for these three runs. The dotted line is for  $N = 9$  and  $c_1 = 2.0$

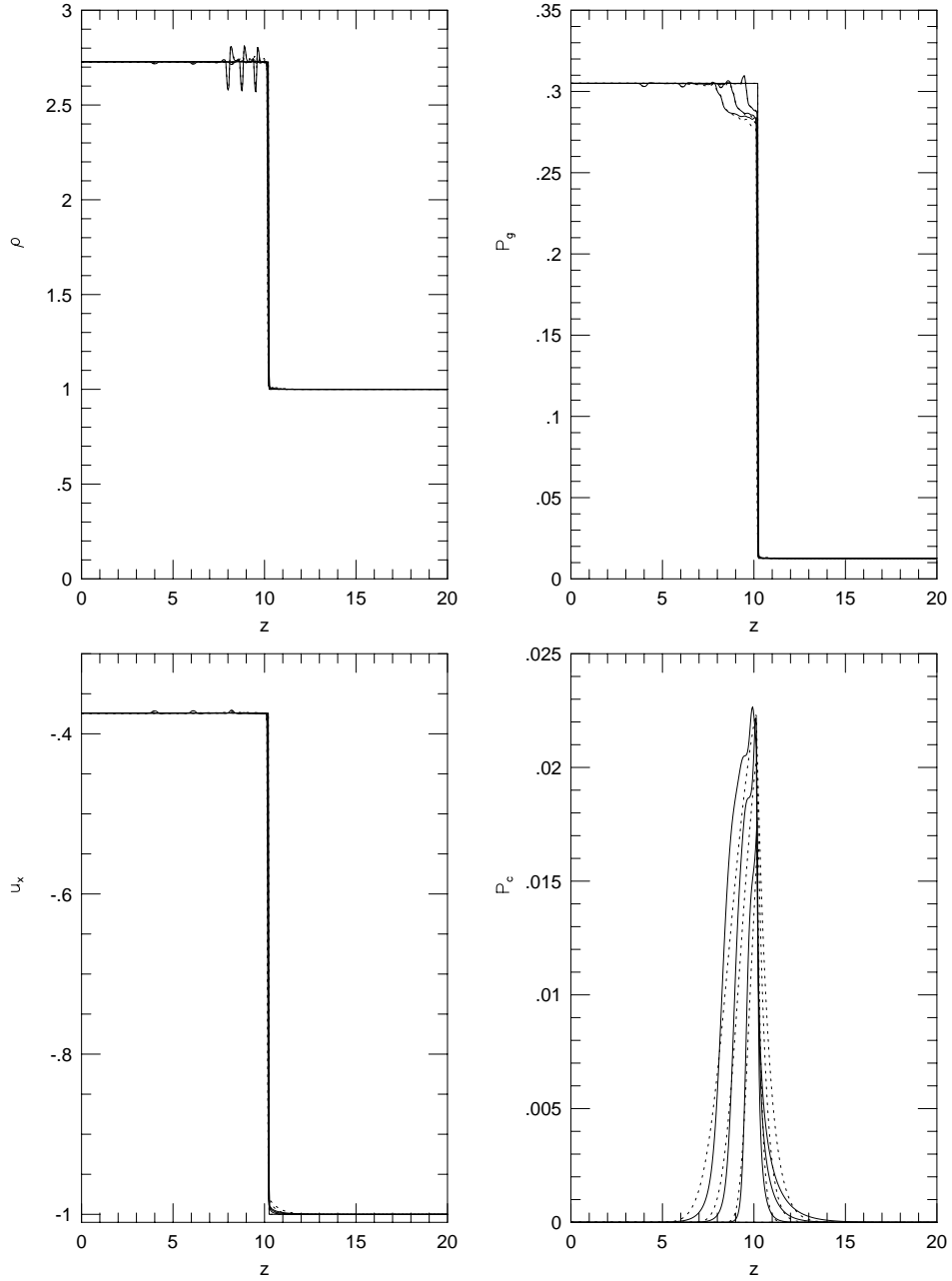


Fig. 6.— The shock structure computed for the *BOEF95-1* shock at  $t = 2, 4, 6$  minutes. The diffusion-convection solution is shown by the solid lines and the two-fluid solution by the dotted lines. The two-fluid solution uses a mean diffusion coefficient that evolves in time according to a simple test particle model for the distribution function. The shock initial conditions are indicated by the discontinuous curves. Details are given in the text.

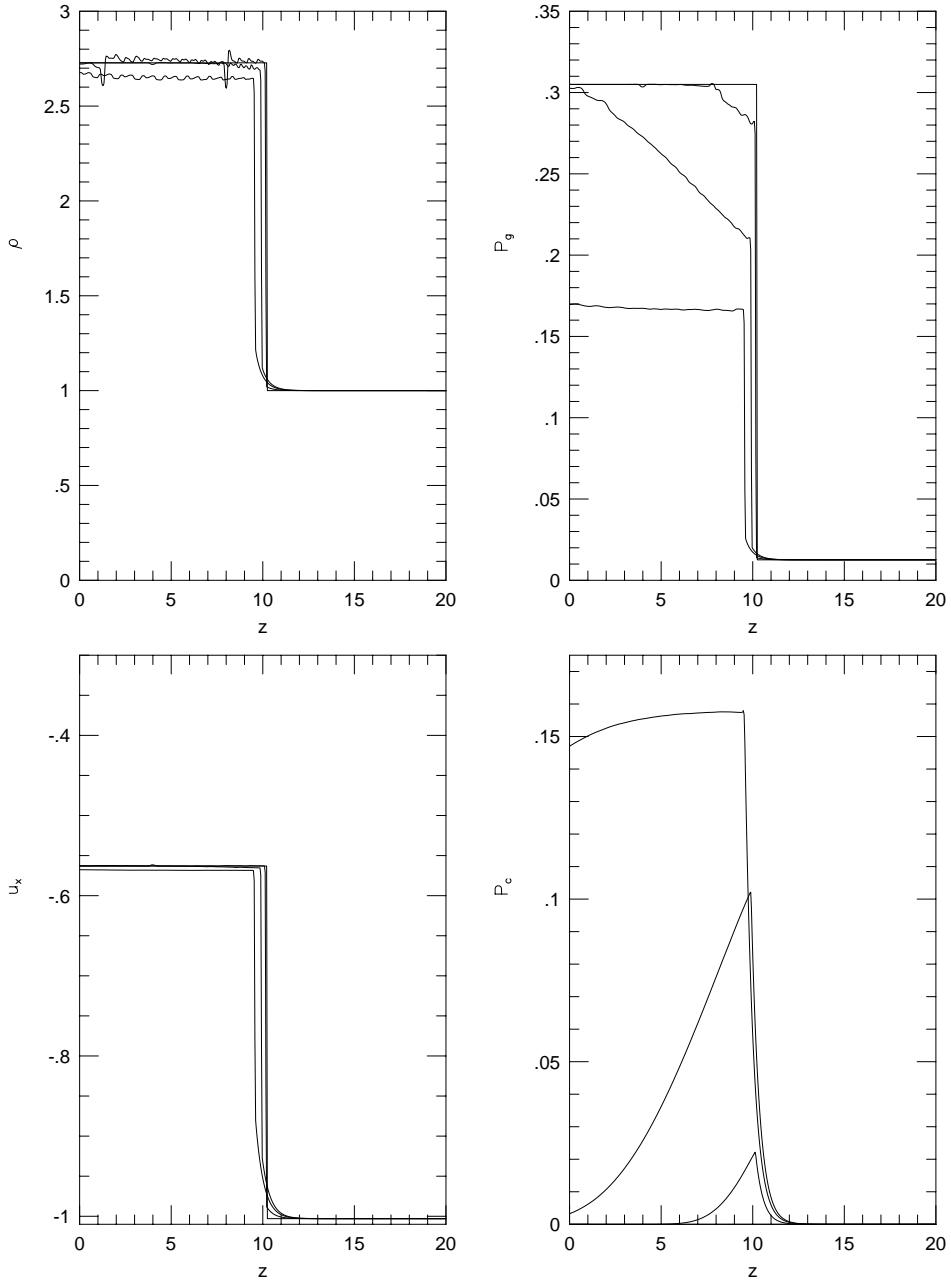


Fig. 7.— Evolution of the shock structure for the shock *BOEF95-1C*. This is a two-fluid model shock and differs from the two-fluid shock shown in Fig. 6 only in the use here of a constant diffusion coefficient,  $\langle \kappa \rangle = 0.4$ . Times represented are  $t = 0, 6, 24, 72$ . For the last time the shock has approached its time-asymptotic limit.